

## Characteristics of fluctuating lift forces of a circular cylinder during generation of vortex excitation

Sangil Kim<sup>†</sup> and Hiroshi Sakamoto<sup>‡</sup>

*Department of Mechanical Engineering, Kitami Institute of Technology,  
165 Koen-cho, Kitami, Hokkaido 090-8507, Japan*

*(Received June 24, 2005, Accepted February 3, 2006)*

**Abstract.** This paper describes the characteristics of the fluctuating lift forces when a circular cylinder vibrates in the cross-flow direction. The response characteristics on elastically supported the circular cylinder was first examined by a free-vibration test. Next, flow-induced vibrations obtained by the free-vibration test were reproduced by a forced-vibration test, and then the characteristics of the fluctuating lift forces, the work done by the fluctuating lift, the behavior of the rolling-up of the separated shear layers were investigated on the basis of the visualized flow patterns. The main findings were that (i) the fluctuating lift forces become considerably large than those of a stationary circular cylinder, (ii) negative pressure generates on the surface of the circular cylinder when the rolling-up of separated shear layer begins, (iii) the phase between the fluctuating lift force and the cylinder displacement changes abruptly as the reduced velocity  $U_r$  increases, and (iv) whether the generating cross-flow vibration becomes divergent or convergent can be described based on the work done by the fluctuating lift force. Furthermore, it was found that the generation of cross-flow vibration can be perfectly suppressed when the small tripping rods are installed on the surface of the circular cylinder.

**Keywords:** circular cylinder; cross-flow vibration; vortex excitation; fluctuating fluid forces; displacement; separated shear layers; phase.

---

### 1. Introduction

It is well known that a flow passing over a circular cylinder may cause both in-line vibration in the stream-wise direction and cross-flow vibration in the direction normal to the flow. The in-line vibration occurred a circular cylinder is also divided into two types by the difference of vortex patterns formed behind the cylinder, which are the Karman vortex and the twin vortex. Furthermore, flow-induced vibration in the cross-flow direction which is called vortex excitation is induced by fluctuating lift caused by the Karman vortex. The present study describes the phenomenon of vortex excitation of a circular cylinder during cross-flow vibration. Numerous studies have been conducted on vortex excitation of a circular cylinder due to its importance in engineering. There are research done on the response characteristics of vortex excitation mounted elastically (Anagnostopoulos and Bearman 1992, Brika and Laneville 1993, Okajima, *et al.* 1999), the characteristics of vortex

---

<sup>†</sup> E-mail: [ksi311@hanmail.net](mailto:ksi311@hanmail.net)

<sup>‡</sup> Professor, Corresponding Author, E-mail: [sakamoto@mech.kitami-it.ac.jp](mailto:sakamoto@mech.kitami-it.ac.jp)

shedding (Ongoren and Rockwell 1988, Griffin and Ramberg 1974, Williamson and Roshko 1988, Gu, *et al.* 1994) and the characteristics of fluid forces acting on a circular cylinder (Hover, *et al.* 1998, Bishop and Hassan 1964, Khalak and Williamson 1999, Moe and Wu 1990, Shiels and Roshko 2001, Carberry, *et al.* 2001, Govardhan and Williamson 2000, Okamoto, *et al.* 2001) when vortex excitation occurs. Much research related with vortex excitation during cross-flow vibration has been carried out and then such research has considerably clarified the response characteristics of flow-induced vibration, vortex shedding and fluid forces. However, the majority of studies of vortex shedding and fluid forces when the cylinder is vibrating have been carried out under conditions of forced vibration at fixed amplitudes. There have been relatively few studies that have accurately reproduced the vibration characteristics of vortex excitation and examined the characteristics of fluid forces and vortex shedding. Govardhan and Williamson (2000) have recently performed a free-vibration test examining in detail the flow added mass for vortex excitation and the influence of the vibration damping ratio, in addition to measuring the vorticity and fluid forces. Their study, however, does not go into the characteristics of the fluctuating fluid forces that induce vortex excitation, the relation between the behavior of shear layers separated from the cylinder and the characteristics of the vibration response. In short, there are still many unclear issues concerning vortex excitation vibrating in the direction perpendicular to the flow and the mechanism behind its occurrence. In this study, vortex excitation behavior obtained from a free-vibration test in which a cylinder was elastically mounted was reproduced accurately by a forced-vibration test, and the characteristics of fluctuating lift were examined. Moreover, fluctuating pressure distribution on the cylinder surface at each vibration displacement, the behavior of shear layers separated from circular cylinder surfaces, and the work done by fluctuating lift forces were also investigated. As a result, the mechanism inducing vortex excitation was clarified when the cylinder is vibrating in the cross-flow direction. In addition, a simple method in which tripping rods were installed on the cylinder surface for suppressing flow-induced vibration was tested.

## 2. Experimental materials and methods

The tests were carried out in a closed-circuit rectangular wind tunnel 0.35 m wide, 1.2 m high and 3 m long, and in a recirculating water channel for visualization with a test section of 30 cm in width, 40 cm in depth and 2 m in length. The diameter of the circular cylinder used the free vibration test was 67 mm. In order to make the cylinder as light as possible, it was constructed with polyurethane covered with a 0.2 mm aluminum plate. The shaft supporting the cylinder constructed from aluminum pipe 10 mm in diameter. The support shaft of the test cylinder was secured at both ends with support assemblies outside of the wind tunnel, as shown in Fig. 1. Each support assembly of the test cylinder consisted of two leaf springs 0.3 mm thick (phosphor bronze) at the top and bottom, and two coil springs, allowing for free vertical (cross-flow) vibration. The vibration displacement of the cylinder was measured by a laser displacement meter. The reduced velocity  $U_r$ , [ $= U_0/(f_c \cdot D)$ ;  $U_0$ : velocity of flow;  $f_c$ : natural frequency of circular cylinder] was varied, but the reduced mass-damping factor  $Cn$  [ $= 2m\delta/(\rho D^2)$ ;  $m$ : mass of cylinder;  $\delta$ : the logarithmic decrement;  $\rho$ : density of fluid;  $D$ : diameter of cylinder] was kept constant. In order to test the suppression of vortex excitation, a control method using tripping rods that has proven extremely effective in suppressing fluid forces in the authors' previous studies was applied (Tan, *et al.* 2003), and the presence or absence of vortex excitation was examined in the free-vibration test. Next, a forced-vibration test was performed by using the vibration device shown in Fig. 2. This arrangement

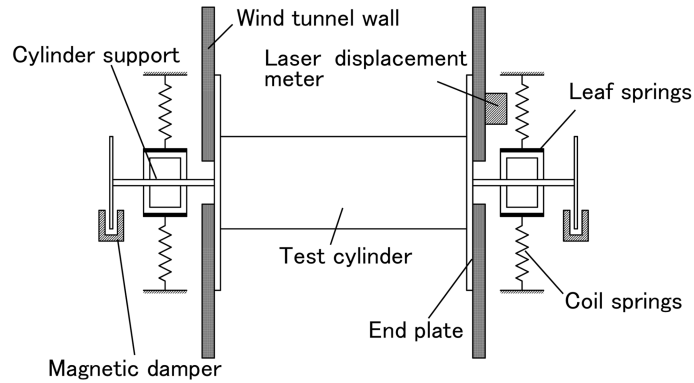


Fig. 1 View of free vibration experimental equipment

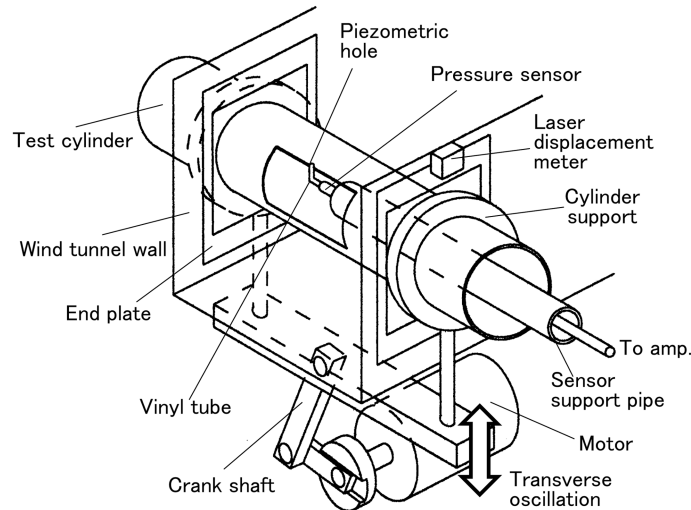


Fig. 2 View of forced vibration experimental equipment

oscillated the test cylinder to move up and down with the rotation of the motor via the crankshaft, and also made it possible to change the amplitude at will. In the forced vibration test, a hollow aluminum cylinder of 100 mm in diameter was used. There was a pressure transducer (piezometer) in the cylinder to measure the pressure on the surface of the cylinder. The piezometer, which was connected to the hole by a silicon tube, was contained in the cylinder but installed in a hollow 16 mm diameter hollow pipe isolated from the cylinder in order to eliminate the influence of the cylinder vibration. The pressure transducer had a gain factor of  $1 \pm 0.05$  in the 0~400 Hz range, and there was very little phase difference in response to changes in frequency. The vibration amplitude and reduced velocity obtained from the free-vibration test were reproduced accurately in the forced-vibration test, and the fluctuating pressure on the cylinder surface was obtained as an ensemble-averaged method in which the vibration displacement of the cylinder or the waveform of fluctuating velocity in the wake was adopted as a reference signal. The fluctuating lift of the cylinder and the work done by fluctuating lift were calculated based on the fluctuating pressure from the ensemble-

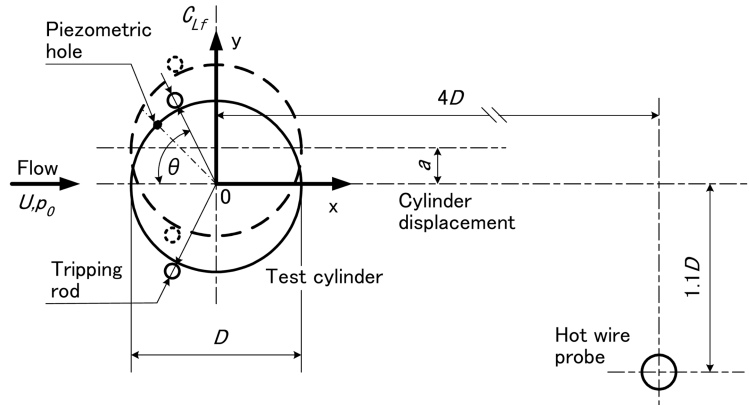


Fig. 3 Coordinate system and definition of symbols

averaged. The Reynolds number in the forced-vibration was  $4.9 \times 10^4$  in the wind tunnel test, which is below the sub-critical Reynolds number. In order to visualize the flow around the cylinder in the water channel test, sodium fluorescein and hydrogen bubbles were used. The main flow velocity was from 1.0 cm/s to 2.0 cm/s, with a Reynolds number from 500 to 1400. Though the Reynolds numbers were quite different between the wind tunnel and water channel tests, it was judged that this difference would not adversely affect a qualitative evaluation of the flow. This is described in more detail in section 4.3 below. Fig. 3 shows the coordinate system and definition of symbols in this test.

### 3. Results and discussion

#### 3.1. Suppression and response characteristics of cross-flow vibration of the cylinder

Fig. 4 shows the response characteristics of cross-flow vibration obtained by the free-vibration test. As shown in the figure, vortex excitation occurs around the reduced critical velocity  $U_{rc} [= U_0 / (f_v \cdot D)]$ , which is consistent with the results of previous research (Okajima, *et al.* 1999). In addition, the vortex shedding frequency was synchronous with the natural frequency ( $f_c$ ) of the cylinder during vortex excitation. In the present study, the vibration amplitude and reduced velocity obtained by the free-vibration test were reproduced accurately in a forced-vibration test, and from these results an evaluation was carried out of the mechanism generating vortex excitation and the characteristics of the fluctuating fluid forces. The following describes the method and results of the vortex excitation suppression test. The authors have previously demonstrated that tripping rods (10% of cylinder diameter) installed at  $\pm 30^\circ$  to  $\pm 40^\circ$  from the stagnation point can almost completely suppress vortex generation in the wake of the cylinder in addition to fluctuating fluid forces (Tan, *et al.* 2003). The results of the application of this suppression method in the free vibration test are also shown in Fig. 4. In this case, the tripping rods ( $d = 6$  mm,  $d/D = 0.09$ ) were installed  $\pm 40^\circ$  from the stagnation point on the cylinder surface. As can be seen in Fig. 4, the generation of vortex excitation causing cross-flow vibration was completely suppressed by the tripping rods. Fig. 5 shows the spectrum results of fluctuating velocity in the wake of the cylinder both with and without tripping rods installed. In the figure,  $f_n$  indicates the vortex shedding

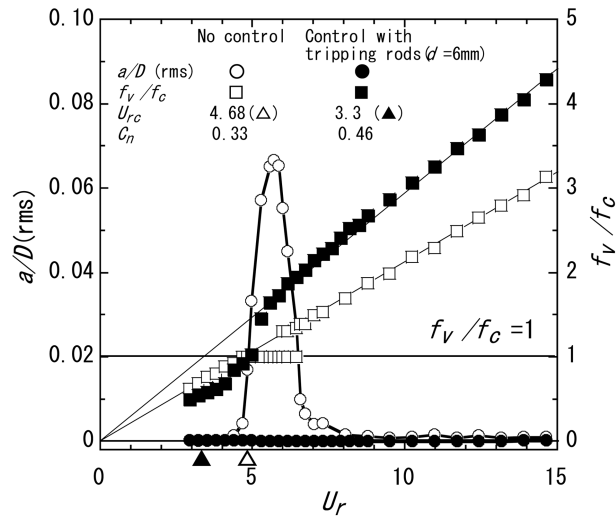


Fig. 4 Response characteristics of circular cylinder with cross-flow vibration

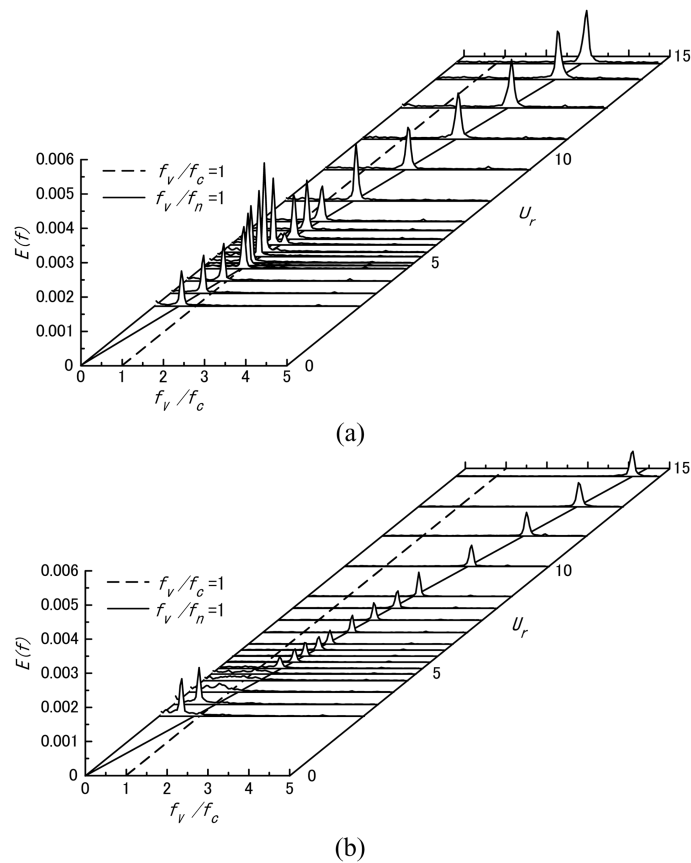


Fig. 5 Power spectrum of fluctuating velocity in wake behind circular cylinder. (a) No control and (b) Control with tripping rods( $d=6$  mm)

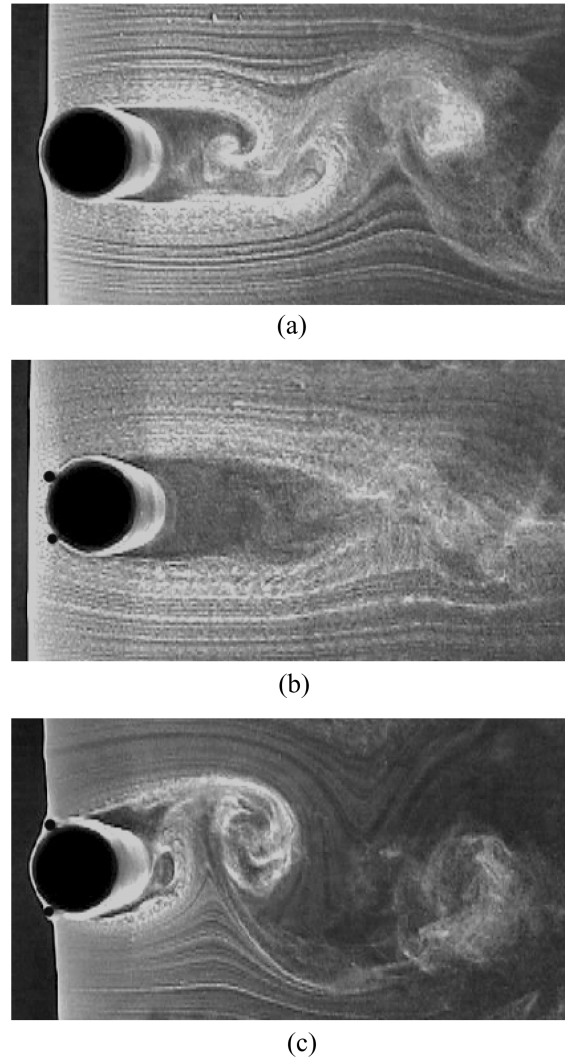


Fig. 6 Visualized flow patterns of circular cylinder with and without and without tripping rods. (a) Without tripping rods, (b) With tripping rods( $\theta=40^\circ$  set up), and (c) With tripping rods( $\theta=60^\circ$  set up)

frequency when the cylinder is stationary. There is still a peak in the spectrum when the tripping rods are installed, but the value of energy is considerably smaller than that without the rods. Fig. 6 shows the flow patterns around the cylinder both without and with tripping rods installed ( $Re \doteq 1400$ ,  $d/D=0.1$ ). When the tripping rods are installed at  $\pm 40^\circ$ , the Karman vortex is almost completely suppressed, and it corresponds well with suppression results of vortex excitation shown in Fig. 4. In addition, when rods are attached, the peaks in the spectrum as shown in Fig. 5 are not a Karman vortex street, but an undulation in the wake of a cylinder, as is clear from the visualization results shown in Fig. 6(b). However, when the tripping rods are installed at  $\pm 60^\circ$ , a Karman vortex street much larger than with no control is generated, which is assumed to cause the likewise larger excitation induced. Therefore, the optimal place for the tripping rods in order to

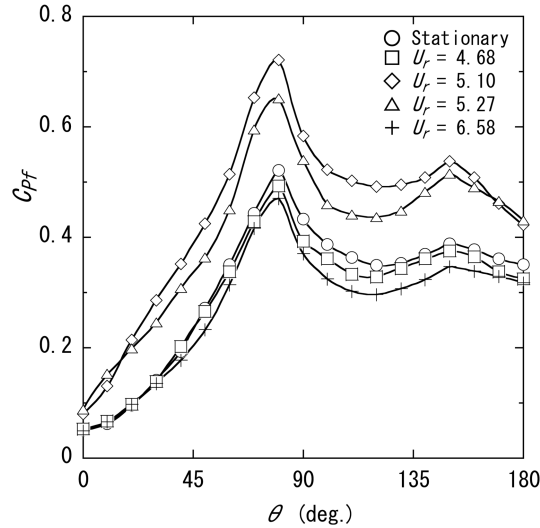


Fig. 7 Fluctuating pressure distributions on surface of circular cylinder

suppress vortex excitation is the considerably limited position around  $40^\circ$ . As is clear from the above, this method for suppressing vortex excitation which induces cross-flow vibration in a cylinder was found to be extremely effective.

### 3.2. Characteristics of fluctuating lift in cross-flow vibration

Fig. 7 shows the pressure distributions of the cylinder surface in the forced-vibration test when the vibration characteristics obtained by the free-vibration test was reproduced. Fluctuating pressure distribution coefficients  $C_{pf}$  (RMS) are shown for:  $U_r = 4.68$  at which vortex excitation starts,  $U_r = 5.27$  at which vibration amplitude reaches maximum,  $U_r = 6.58$  at which vortex excitation converges, and  $U_r = 5.10$  at which fluctuating pressure reaches maximum. Fluctuating pressure distribution for a stationary cylinder is also shown in this figure for comparison purposes. Values of  $C_{pf}$  for  $U_r = 4.68$  and  $U_r = 6.58$  at which vibration starts and converges, respectively, are slightly smaller than those when the cylinder is stationary. This is due to the rolling-up of the Karman vortex becoming weak because there exists both the non-lock-in and lock-in patterns where vibration starts and converges. On the other hand, the  $C_{pf}$  values at  $U_r = 5.10$  and  $5.27$ , where the cylinder sheds vortices at its natural frequency, or lock-in, were considerably higher than those when the cylinder is stationary, meaning that the rolling-up of the Karman vortex during lock-in conditions becomes considerably stronger. Next, Fig. 8 shows the fluctuating lift coefficient  $C_{Lf}$  (RMS) at each  $U_r$  when vibration characteristics obtained from the free-vibration tests shown in Fig. 4 were reproduced by forced-vibration tests. The  $C_{Lf}$  values shown in Fig. 8 were calculated based on the fluctuating pressure coefficient  $\{C_{pf}(j)\} = \{p_f(j)\} / (0.5\rho U_0^2)$ , which was obtained by ensemble-averaged method using the vibration displacement of the cylinder or fluctuating velocity in the wake as a reference signal. For measuring the ensemble-averaged value  $\{C_{pf}(j)\}$  of the fluctuating pressure, the number of calculations  $j$  was 200 to 300. It is clear from the figure that the  $C_{Lf}$  reaches maximum at  $U_r = 5.10$ . The  $C_{Lf}$  is much larger than that of a stationary cylinder. But this  $U_r$ , at which the value of  $C_{Lf}$  reaches maximum, differs from the  $U_r (= 5.27)$  at which the amplitude

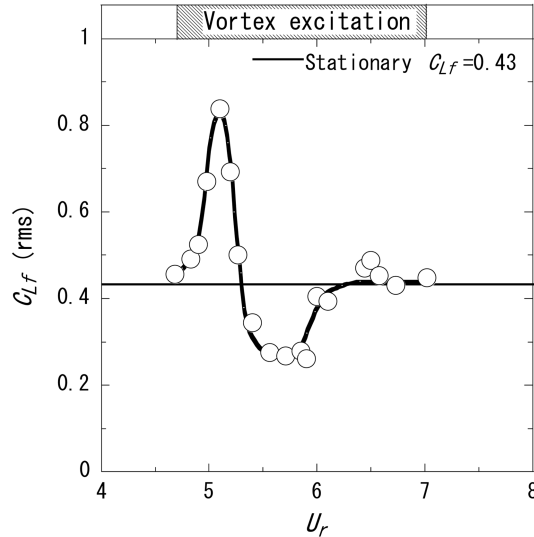


Fig. 8  $C_{L_f}$  values versus  $U_r$

is maximum. This is because the  $U_r$  at which the work done by the fluctuating lift which induces the vibration is different from the  $U_r$  at which  $C_{L_f}$  becomes maximum due to a change in phase between the generation of fluctuating lift and vibration displacement depending on  $U_r$ . This is described in more detail in 4.5 below. Furthermore, the value of  $C_{L_f}$  is much smaller than that of a stationary cylinder when  $U_r$  exceeds 5.30. This is because the rolling-up of the Karman vortex becomes weak due to there being two vortex shedding patterns (non-lock-in and lock-in) when  $U_r$  exceeds 5.30.

### 3.3. Relationship between vibration displacement and fluctuating fluid force

Fig. 9 shows fluctuating pressure distributions on the circular cylinder surface at each phase  $\varphi$  of vibration displacement through one period of vibration at each of the four reduced velocities  $U_r$ . The four  $U_r$  reduced velocity values shown in the Fig. 9 correspond to the vibration response characteristics as shown in Fig. 4: that of 4.68 at which the vibration starts, 5.27 at which the vibration amplitude reaches maximum, 5.10 at which the fluctuating lift reaches maximum, and 6.58 at which the vibration converges. The relationship between the behavior of shear layers and the fluctuating lift with a stationary circular cylinder has already been clarified by Sarpkaya (1979). When the shear layers separate around  $\theta = 90^\circ$  ( $\theta$  is the angle from the stagnation point when the right rotation is positive) on the circular cylinder surface, fluctuating lift is generated upward. Conversely, when the shear layers separate around  $\theta = -90^\circ$  on the circular cylinder surface, the fluctuating lift is generated downward. The largest amount of fluctuating lift is generated around  $\varphi = \pi/2$ , in the middle of where the rolling-up of the shear layer ceases. It has already been clarified that there is a clear relationship between the rolling-up behavior of the shear layers separated from circular cylinders and the fluctuating lift. The fluctuating pressure distributions on the vibrating circular cylinder surface at each phase changes dramatically with changes in  $U_r$ , as shown in Fig. 9, and it can be reasoned that phase at which the rolling-up of the shear layers from the surface of the

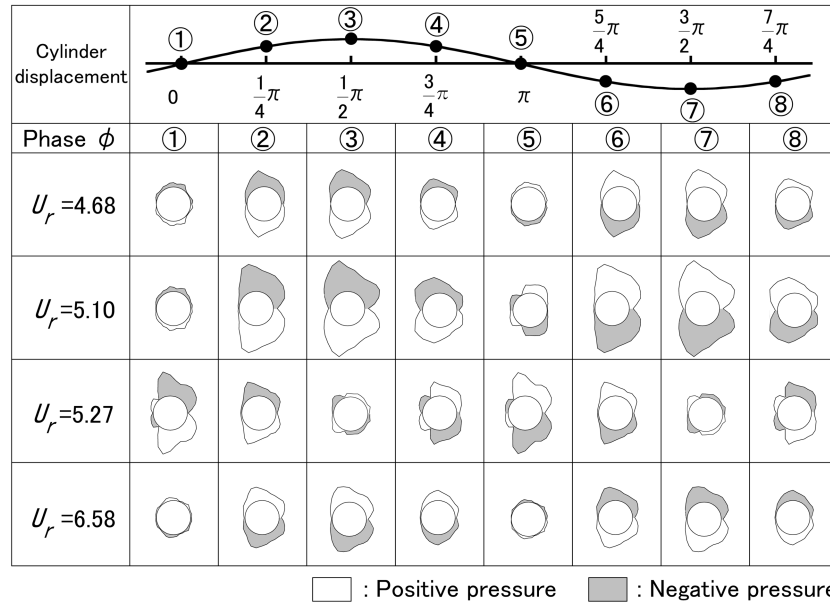


Fig. 9 Fluctuating pressure distributions on surface of cylinder versus one cycle of displacement

circular cylinders changes drastically with the change in  $U_r$ . To confirm this, visualization of the behavior of the shear layers during vibration of the cylinder at  $U_r = 4.68, 5.27$  and  $6.58$  was performed. These results are shown in Fig. 10. In this visualization test, the Reynolds number was around 500, and in the wind tunnel test, the Reynolds number was  $4.9 \times 10^4$ . Although these two Reynolds numbers are very different, both are equivalent in that the separated shear layers and vortex in the wake become turbulent (the laminar shear layers separated from the cylinder become a turbulent Karman vortex in the range of  $260 < Re < 3.5 \times 10^5$ ) at the same place (Zdravkovich 1997), and the laminar boundary layer on the surface of the cylinder separates at  $\theta = 90^\circ$ , meaning that a qualitative evaluation can be carried out with no significant problems. Below is a discussion in which the fluctuating pressure distributions on the cylinder surface shown Fig. 9 and the rolling-up behavior of the separated shear layers shown in Fig. 10 are compared. The mechanism that generates fluctuating lift is examined for three  $U_r$ . First, in the vicinity of  $U_r = 4.68$  where vibration starts, when the circular cylinder approaches the top dead point (where the vibration displacement phase  $\phi$  is  $\pi/2$ ) at  $\phi = 0$ , the shear layers begin to separate at  $\theta = 90^\circ$  on the circular cylinder surface, and negative fluctuating pressure on the upper surface of the circular cylinder begins to be generated. When the cylinder reaches the top dead point, the fluctuating pressure reaches at maximum. When the cylinder approaches the bottom dead point at  $\phi = 3\pi/2$  from  $\phi = \pi/2$ , the shear layers develop into a large-scale vortex, but the fluctuating pressure on the cylinder surface gradually decreases, becoming almost zero near  $\phi = \pi$ . The shear layers separated from the top of the cylinder ( $\theta = 90^\circ$ ) develop into a large vortex, and beginning to shed the Karman vortex near  $\phi = \pi$ . Next, when the cylinder approaching the bottom dead point from  $\phi = \pi/2$  passes the point around  $\phi = \pi$ , the shear layers begin to roll up from the bottom of the cylinder ( $\theta = -90^\circ$ ), and negative fluctuating pressure begins to be generated on the bottom of the cylinder surface. The fluctuating pressure reaches maximum when the cylinder reaches the bottom dead point. As

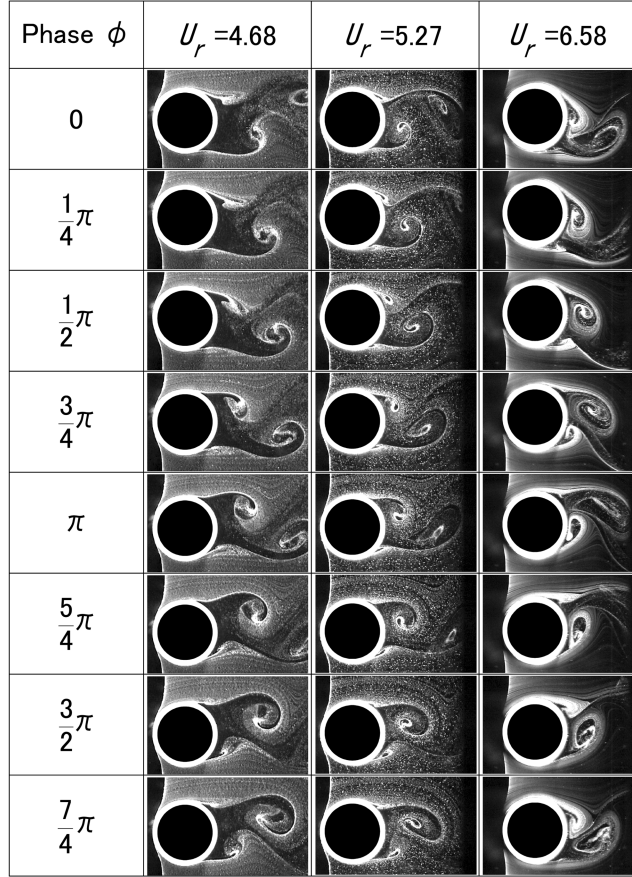


Fig. 10 Visualized observation of rolling-up separated shear layers

described above, at  $U_r = 4.68$  at which vibration starts, when the cylinder approaches the top dead point at  $\phi = 0$  and approaches the bottom dead point at  $\phi = \pi$ , the shear layers begin to separate and begin to roll up at top and bottom of the cylinder ( $\theta = \pm 90^\circ$ ). The fluctuating pressure also increases together with the development of the shear layers, and maximum fluctuating pressure is generated at  $\phi = \pi/2$  and  $\phi = 3\pi/2$ . Though not shown in Fig. 10, the rolling up of the shear layers at  $U_r = 5.10$ , at which the fluctuating pressure becomes maximum as shown in Fig. 9, exhibits almost the same behavior as  $U_r = 4.68$  at which vibration starts. However, compared to  $U_r = 4.68$ , the rolling up of the shear layers is stronger due to the higher vibration amplitude at  $U_r = 5.10$ ; therefore the fluctuating pressure generated becomes considerably larger. This results in the largest generation of fluctuating lift. Next, at  $U_r = 5.27$  at which the vibration amplitude becomes maximum, the separated shear layer from the  $\theta = 90^\circ$  point on the top of the cylinder starts to roll up when the cylinder begins to approach the top dead point from the bottom dead point at around  $\phi = 3\pi/2$ , and the negative fluctuating pressure on the upper cylinder surface reaches maximum at  $\phi = 0$ . As is clear from the above, the phase at which the separated shear layers begin to roll up on the top and bottom of the cylinder at  $U_r = 5.27$  deviates by  $\pi/2$  in comparison with that of  $U_r = 4.68$ . As a result, the phase of fluctuating pressure generation also deviates by exactly  $\pi/2$  as well with respect

to vibration displacement. In addition, at around  $U_r = 6.58$ , where the vibration of the circular cylinder converges, the separation of the shear layers begins at the bottom of the circular cylinder at around  $\phi = 0$ , where the displaced cylinder approaches the top dead point. Therefore, the fluctuating pressure generation deviates in comparison with that of  $U_r = 4.68$  by precisely  $\pi$  as well, which is the opposite phase. As a result, the phase of fluctuating lift generation on the circular cylinder likewise deviates by  $\pi$ .

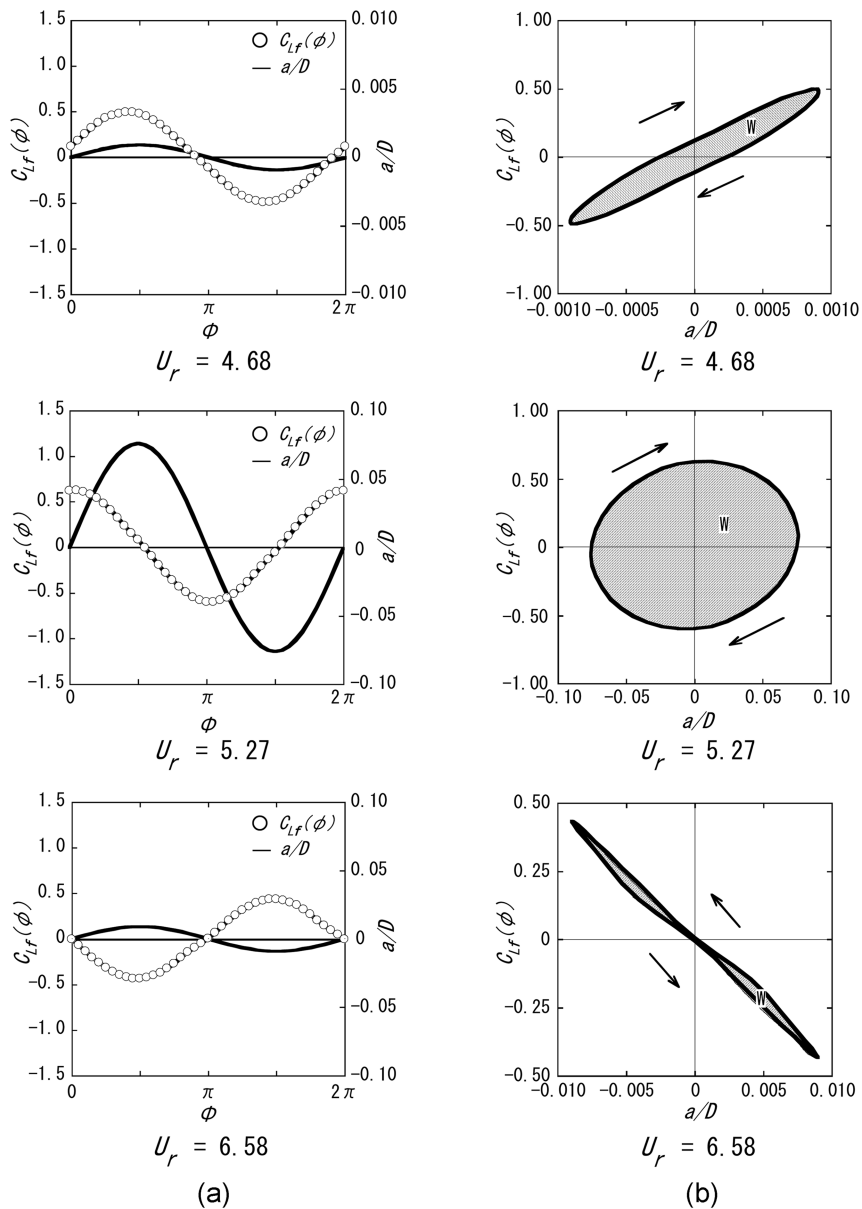


Fig. 11 Relationship between fluctuating lift and vibration displacement. (a) Change of fluctuating lift for displacement  $a/D$  and (b) Lissajous' diagram based on  $C_{L_f}(\phi)$  and  $a/D$

### 3.4. Phase between fluctuating lift and vibration displacement

Fig. 11(a) shows the fluctuating lift of a cylinder at  $U_r = 4.68, 5.27$  and  $6.58$  for one period of vibration, in addition to the vibration displacement of the cylinder. As described for fluctuating pressure distributions shown in Fig. 9, the start of the generation of the upward fluctuating lift is at  $\varphi = 0$  when  $U_r$  is 4.68. The phases at  $U_r = 5.27$  and  $6.58$  deviate by  $\pi/2$  and  $\pi$  respectively in comparison. Fig. 12 shows the phase where the upward fluctuating lift is generated on the basis of  $\varphi = 0$  at which the vibration displacement is zero when the cylinder approaches the top dead point: in other words, this is the phase difference  $\varphi_d$ . When a  $U_r$  of 5.10 is exceeded, the phase difference  $\varphi_d$  at which upward fluctuating lift begins to arise increases rapidly, becoming almost  $\pi/2$  when  $U_r = 5.27$  and almost  $\pi$  when  $U_r = 6.10$ . This phase difference  $\varphi_d$  of fluctuating lift with an increase in the  $U_r$  is based on the change of the phase in which rolling-up of the shear layer separated from the circular cylinder starts, as described in section 4.3. Okamoto (2001), Govardhan and Williamson (2000), and Bearman-Currie (1979) have also examined the difference of phase between vibration displacement and fluctuating lift of a circular cylinder that vibrates in the cross-flow direction. The tendencies shown by them are nearly identical to the present results, as shown in Fig. 12. It is notable that the phase in which fluctuating lift is generated at limited  $U_r$  region where the vortex excitation is generated, or to put it differently, the phase in which the shear layer separated from the circular cylinder surface begins to roll up changes from 0 to  $\pi$ . At present, however, it is not certain what kind of mechanism this change is based on.

### 3.5. The work $W$ done by fluid

Fig. 11(b) shows a Lissajous figure which is calculated on the basis of fluctuating lift and vibration displacement for one period. With this Lissajous figure, it is possible to evaluate both the damping and excitation in vortex-induced vibration by the work  $W$  which the fluid does on the

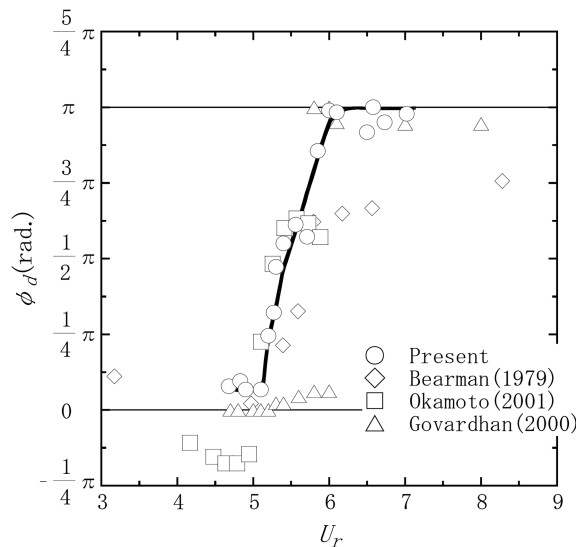


Fig. 12 Phase shift between fluctuating lift and cylinder displacement

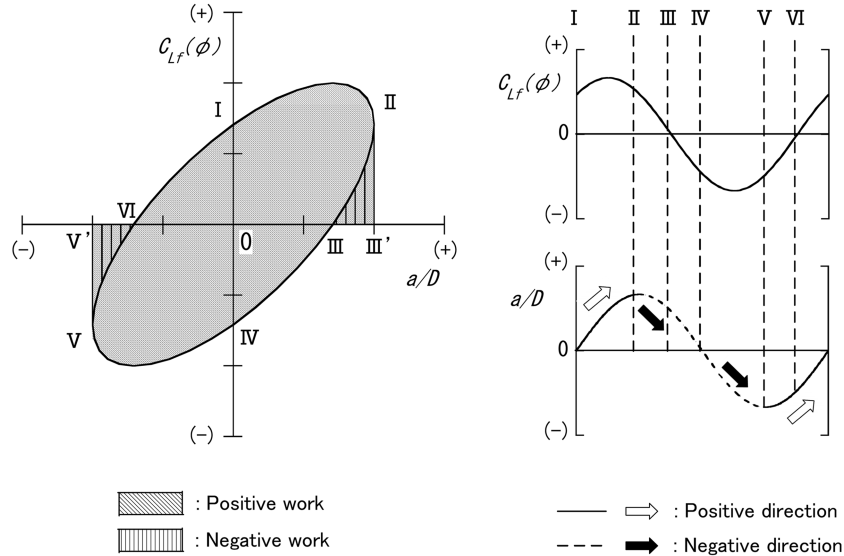


Fig. 13 Relationship between Lissajous figure and work  $W$

cylinder. Specifically, the work  $W$  which the fluctuating lift does on the cylinder is as follows:

$$W = \int_{-a}^a C_{L_f}(\phi) \times d(a/D) \tag{1}$$

The solution of the above equation is the area of the Lissajous figure in Fig. 11(b). To explain this in more detail, Fig. 13 shows the relation between the Lissajous figure and work on the basis of  $C_{L_f}(\phi)$  and  $a/D$ . The ordinate is the fluctuating lift  $C_{L_f}(\phi)$  and the abscissa is the vibration amplitude  $a/D$ . The upper direction is positive with  $C_{L_f}(\phi)$  and  $a/D$ . Points I to VI correspond with each position in Fig. 13. To begin with, in the region of I to II, the work area bounded by 0, I, II, and III' is positive since the directions of both  $C_{L_f}(\phi)$  and  $a/D$  are the same. But the work area bounded by II, III', and III is negative since  $C_{L_f}(\phi)$  and  $a/D$  are of the opposite direction in the region of II to III. Furthermore, the work area bounded by 0, III, and IV is positive since both  $C_{L_f}(\phi)$  and  $a/D$  are of the same direction in the region of III to IV. Consequently, only the area bounded by I, II, III, and IV of positive work remains in the right half of the Lissajous figure since the area bounded by II, III', and III is cancelled out. Also, only the area of positive work bounded by I, IV, V, and VI remains in the left half of the Lissajous figure. Therefore, the work is calculated so that the clockwise rotation of the Lissajous figure represents positive work and the counter-clockwise direction represents negative work. Fig. 14 shows the work  $W$  which the fluid does on the cylinder based on  $C_{L_f}(\phi)$ . This means that when vortex excitation begins to be generated, the work  $W$  becomes positive and the fluid makes the cylinder vibrate. The work  $W$  reaches maximum near  $U_r = 5.27$  at which the vibration amplitude reaches maximum. If  $U_r$  exceeds 5.27, the work  $W$  decreases, approaching zero near  $U_r = 6.0$ . Furthermore, if  $U_r$  exceeds 6.0, the work  $W$  becomes negative, and the fluid therefore makes the cylinder vibration converge. As shown above, there is a clear correspondence between the work  $W$  done by the fluid and the vibration amplitude of the cylinder. We can assume that the vibration is either convergent or divergent by evaluating the work  $W$ , and this is one effective method towards clarifying the mechanism generating flow-induced vibration.

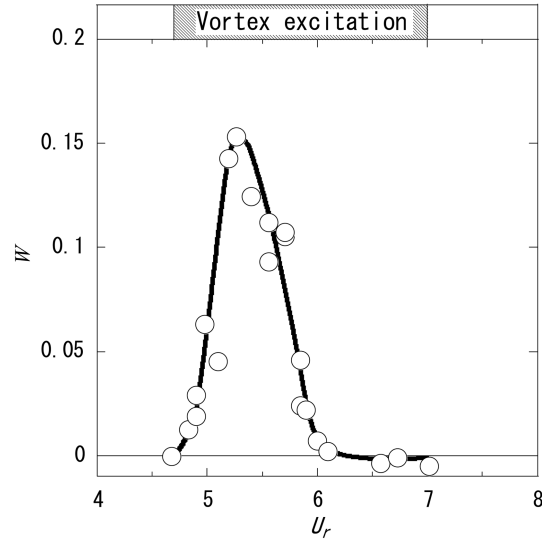


Fig. 14 Work done by fluctuating lift versus  $U_r$

#### 4. Conclusions

- (1) Cross-flow vibration of the cylinder is generated near the reduced critical velocity  $U_{rc}$ , and the response characteristics are the same as those indicated in numerous previous studies. In addition, cross-flow vibration can be suppressed by using tripping rods with a diameter 10% of the cylinder installed at  $\pm 40$  degrees on the cylinder surface from the stagnation point.
- (2) The characteristics of the fluctuating fluid force were examined by correspondence to vibration amplitude generated in the cylinder. It was found that the fluctuating lift considerably increases with an increase in vibration amplitude. However, the position of  $U_r$  in which the largest fluctuating lift arises is not the same as that in which the largest vibration amplitude arises.
- (3) A clear relation was established between fluctuating pressure on the circular cylinder surface and the rolling-up behavior of separated shear layers from the surface at each  $U_r$  in which cross-flow vibration is generated.
- (4) The phase difference  $\varphi_l$  between displacement of fluctuating lift and vibration displacement changes drastically with a change in  $U_r$ . That is to say, it is zero (i.e., the same phase) at the start of the vibration,  $\pi/2$  at the maximum amplitude, and  $\pi$  at the convergence of the vibration.
- (5) A Lissajous figure was constructed on the basis of fluctuating lift and vibration amplitude, allowing for the evaluation of the work  $W$  done by the fluid. Finally, it is shown that there is a clear correspondence with the work  $W$  done by the fluid at each  $U_r$  and the vibration amplitude of the cylinder.

#### Notation

- $a$  : vibration amplitude in the cross-flow direction  
 $C_{Lf}$  : coefficient of fluctuating lift force (RMS)  
 $C_{Lf}(\varphi)$  : coefficient of fluctuating lift force in one period

$Cn$	: reduced mass-damping factor [= $2m\delta/(\rho \cdot D^2)$ ]
$\langle C_{pf} \rangle$	: ensemble-averaged fluctuating pressure
$d$	: tripping rod diameter
$D$	: test cylinder diameter
$f_c$	: natural frequency of the cylinder
$f_v$	: vortex shedding frequency from the cylinder
$p_f$	: fluctuating pressure on the cylinder surface
$p_0$	: static pressure of flow
$U_0$	: velocity of flow
$U_r$	: reduced velocity [= $U_0/(f_c D)$ ]
$U_{rc}$	: reduced critical velocity [= $U_0/(f_v D)$ ]
$W$	: work done by fluctuating lift force [Eq. (1)]
$\delta$	: logarithmic damping ratio
$\theta$	: angle from the stagnation point
$\rho$	: density of fluid
$\varphi$	: phase between $a$ and $C_{L_f}(\varphi)$
$\varphi_d$	: phase difference between fluctuating lift and vibration displacement

## References

- Anagnostopoulos, P. and Bearman, P.W. (1992), "Response characteristics of a vortex-excited cylinder at low Reynolds numbers", *J. Fluids Struct.*, **6**, 39-50.
- Bishop, R.E.D. and Hassan, A.Y. (1964), "The lift and drag forces on a circular cylinder oscillating in a flowing fluid", *Proceedings of the Royal Society of London. Series A*, **277**, 51-75.
- Bearman, P.W. and Currie, I.G. (1979), "Pressure-fluctuation measurements on an oscillating circular cylinder", *J. Fluid Mech.*, **91-4**, 661-677.
- Brika, D. and Laneville, A. (1993), "Vortex-induced vibrations of a long flexible circular cylinder", *J. Fluid Mech.*, **250**, 481-508.
- Carberry, J., Sheridan, J., and Rockwell, D. (2001), "Forces and wake modes of an oscillating cylinder", *J. Fluids Struct.*, **15**, 523-532.
- Govardhan, R. and Williamson, C.H.K. (2000), "Modes of vortex formation and frequency response of a freely vibrating cylinder", *J. Fluid Mech.*, **420**, 85-130.
- Griffin, O.M. and Ramberg, S.E. (1974), "The vortex wakes of vibrating cylinders", *J. Fluid Mech.*, **66**, 553-576.
- Gu, W., Chyu, C., and Rockwell, D. (1994), "Timing of vortex formation from an oscillating cylinder", *Physics Fluids*, **6-11**, 3677-3682.
- Hover, F.S., Techet, A.H., and Triantafyllou, M.S. (1998), "Forces on oscillating uniform and tapered cylinders in crossflow", *J. Fluid Mech.*, **363**, 97-114.
- Khalak, A. and Williamson, C.H.K. (1999), "Motions, forces and mode transitions in vortex-induced vibrations at low mass-damping", *J. Fluids Struct.*, **13**, 813-851.
- Moe, G. and Wu, Z.J. (1990), "The lift force on a cylinder vibrating in a current", *J. Offshore Mech. Arctic Eng.*, ASME, **112**, 297-303.
- Okajima, A., Nagamori, T., Matsunaga, F., and Kiwata, T. (1999), "Some experiments on flow-induced vibration of a circular cylinder with surface roughness", *J. Fluids Struct.*, **13**, 853-864.
- Okamoto, S., Uematsu, R., and Taguwa, Y. (2001), "Fluid force acting on two-dimensional circular cylinder in lock-in phenomenon", *Transactions of the Japan Society of Mechanical Engineers*, **B67-654**, 430-435 (in Japanese).
- Ongoren, A. and Rockwell, D. (1988), "Flow structure from an oscillating cylinder Part 1. Mechanisms of phase shift and recovery in the near wake", *J. Fluid Mech.*, **91**, 197-223.
- Sarpkaya, T. (1979), "Vortex-induced oscillation: A selective review", *Transactions of ASME, J. Appl. Mech.*, **46**,

- 241-258.
- Shiels, A.L. and Roshko, A. (2001), "Flow-induced vibration of a circular cylinder at limiting structural parameters", *J. Fluids Struct.*, **15**, 3-21.
- Tan, K., Moriya, M., and Sakamoto, H. (2003), "Suppression of fluid forces acting on circular cylinder by tripping rods", *Transactions of the Japan Society of Mechanical Engineers*, **B 69-679**, 574-578 (in Japanese).
- Williamson, C.H.K. and Roshko, A. (1988), "Vortex formation in the wake of an oscillating cylinder", *J. Fluids Struct.*, **2**, 355-381.
- Zdravkovich, M.M. (1997), *Flow around Circular Cylinders*, Vol. 1, Oxford University Press.

CC